

# PCCP

Physical Chemistry Chemical Physics

Accepted Manuscript

This article can be cited before page numbers have been issued, to do this please use: L. Meng, F. Viñes and F. Illas, *Phys. Chem. Chem. Phys.*, 2026, DOI: 10.1039/D5CP04556H.



This is an Accepted Manuscript, which has been through the Royal Society of Chemistry peer review process and has been accepted for publication.

Accepted Manuscripts are published online shortly after acceptance, before technical editing, formatting and proof reading. Using this free service, authors can make their results available to the community, in citable form, before we publish the edited article. We will replace this Accepted Manuscript with the edited and formatted Advance Article as soon as it is available.

You can find more information about Accepted Manuscripts in the [Information for Authors](#).

Please note that technical editing may introduce minor changes to the text and/or graphics, which may alter content. The journal's standard [Terms & Conditions](#) and the [Ethical guidelines](#) still apply. In no event shall the Royal Society of Chemistry be held responsible for any errors or omissions in this Accepted Manuscript or any consequences arising from the use of any information it contains.

# Computational Insights into the Structural and Electronic Properties of First-Row Transition Metal-Doped $\text{In}_2\text{O}_3$ Systems

Ling Meng,<sup>ab</sup> Francesc Viñes<sup>a</sup> and Francesc Illas<sup>\*a</sup>

<sup>a</sup> Departament de Ciència de Materials i Química Física & Institut de Química Teòrica i Computacional (IQT-CUB), Universitat de Barcelona, c/ Martí i Franquès 1-11, 08028, Barcelona, Spain.

<sup>b</sup> State Key Laboratory of Chemical Resource Engineering, Beijing Engineering Center for Hierarchical Catalysts, College of Chemistry, Beijing University of Chemical Technology, Beijing 100029, China.

## Abstract

Indium oxide ( $\text{In}_2\text{O}_3$ ) has emerged as a promising catalyst for  $\text{CO}_2$ -to-methanol conversion, although its efficiency is limited by poor  $\text{H}_2$  activation. Inspired by recent findings that economical Co-doping enhances the catalytic performance of  $\text{In}_2\text{O}_3$ , this study employs density functional theory (DFT) to systematically investigate the structural stability and electronic properties of first-row 3d transition metals (TM = Sc, Ti, V, Cr, Mn, Fe, Co, Ni, Cu, Zn) doped  $\text{In}_2\text{O}_3$ , aiming to guide rational catalyst design. The present analysis shows that the electronic configuration of the TM dopant plays a critical role in determining its preferred doping site, formation energy, charge transfer, and electronic distribution. Overall, early transition metals (TMs) exhibit lower formation energies and thus higher thermodynamic stability, whereas late TMs involve higher formation energies. A strong linear correlation between formation energy and Bader charge transfer indicates that electron-donating ability is the dominant factor governing doping stability, whereas the correlation with the *d*-band center is moderate. The analysis of the projected density of states (PDOS) reveals that metals with partially *d* filled orbitals contribute significantly near the Fermi level,  $E_F$ , which may enhance the electron transfer and catalytic activity. In contrast, metals with fully filled *d* orbitals display negligible contribution. This systematic screening of dopants offers a general strategy to enhance  $\text{In}_2\text{O}_3$  catalytic performance and provides a theoretical foundation for the rational design of cost-effective catalysts.

\*corresponding author: [francesc.illas@ub.edu](mailto:francesc.illas@ub.edu)

## 1. Introduction

View Article Online  
DOI: 10.1039/D5CP04556H

The increasing concentration of atmospheric carbon dioxide ( $\text{CO}_2$ ) constitutes a critical issue for both global warming and climate change, which triggered several strategies aimed at mitigating them.<sup>1,2</sup> Carbon capture and utilization (CCU) technologies emerged as a promising approach to use atmospheric  $\text{CO}_2$  as an input feedstock for chemical processes leading to useful chemical commodities such as carbon monoxide (CO), formic acid ( $\text{HCOOH}$ ), and methanol ( $\text{CH}_3\text{OH}$ ),<sup>3-6</sup> which constitute chemical precursors for the synthesis of more complex chemicals and fuels. In particular, methanol, obtained from  $\text{CO}_2$  hydrogenation, is of interest because of its use as a bulk chemical in the industry to produce, among others, olefins, acetic acid, and formaldehyde,<sup>7,8</sup> or as a potential green fuel,<sup>9</sup> provided the used hydrogen is also obtained from green sources.<sup>10,11</sup>

Despite the possible benefit of the direct catalytic hydrogenation of  $\text{CO}_2$  to methanol, a large scale implementation of the process remains hindered because of the  $\text{CO}_2$  high thermodynamic stability and its concomitant problems from the kinetic point of view.<sup>12</sup> Clearly,  $\text{CO}_2$  conversion requires active and, more important, selective catalysts able to conduct the reaction of interest under relatively mild working conditions of temperature and pressure.<sup>13</sup> In this sense, metal oxides<sup>14,15</sup> have attracted considerable attention due to their unique chemistry arising from the presence of different facets and/or of defects such as oxygen vacancies, as elegantly explained by Pacchioni several years ago.<sup>16</sup> Among the vast family of metal oxides, indium oxide ( $\text{In}_2\text{O}_3$ ) is of particular interest because of its ability to selectively catalyze  $\text{CO}_2$  hydrogenation to methanol production, even at rather high working temperatures.<sup>17,18</sup> Nevertheless, some issues still remain as open questions, since Cannizzaro *et al.*<sup>19</sup> demonstrated that, even though  $\text{In}_2\text{O}_3$  exhibits excellent selectivity for methanol by effectively suppressing the competing reverse water-gas shift (RWGS) reaction, the overall  $\text{CO}_2$  conversion remains limited due to the low ability of this oxide to activate and dissociate molecular hydrogen ( $\text{H}_2$ ), which in turn hampers its catalytic efficiency for  $\text{CO}_2$  hydrogenation to methanol.

To overcome the poor performance of  $\text{In}_2\text{O}_3$  towards hydrogen dissociation, several strategies have been explored.<sup>20,21</sup> These involve either metal doping or combining  $\text{In}_2\text{O}_3$  with

other metal oxides.<sup>22</sup> At present, most studies have focused on metal doping because this can enhance catalytic performance by tuning the electronic structure, redox behavior, and defect properties of the material.<sup>23,24</sup> For instance, Dostagir *et al.*<sup>25</sup> reported that Rh-doped  $\text{In}_2\text{O}_3$  exhibits significantly higher  $\text{CO}_2$  conversion and methanol selectivity; while Liu *et al.*<sup>26</sup> showed that a small amount of Pd doping into the  $\text{In}_2\text{O}_3$  enables  $\text{CO}_2$  electroreduction to ethanol with a high Faraday efficiency at a low overpotential, suggesting that the conversion to ethanol is promoted by regulating the adsorption free energy of the CO intermediate. In both examples, expensive scarce metals are employed which claim for more economical and plausible alternatives.

Recently, it has been shown that doping  $\text{In}_2\text{O}_3$  with cobalt (Co) does not only improve the catalytic activity of the host oxide, but also maintains, or even enhances, its selectivity towards methanol.<sup>27,28</sup> To shed light into the effect of Co doping in the properties of  $\text{In}_2\text{O}_3$ , Voccia *et al.*<sup>29</sup> explored the properties of Co-doped  $\text{In}_2\text{O}_3$  combining experimental characterization and density functional theory (DFT) simulations. The authors addressed several key aspects, including the effect of the presence of Co on the crystal lattice and electronic band structure, the oxidation state of Co in the doped system, and the impact of Co on the oxygen vacancy formation energy. More recently, Kapse *et al.* have shown that the presence of Co induces significant changes in the molecular mechanism of  $\text{CO}_2$  hydrogenation, thus explaining the origin of the experimentally observed catalytic activity.<sup>30</sup>

Despite promising results obtained with Co-doped system, a fundamental question remains unresolved; whether other inexpensive 3d transition metals can achieve comparable or superior performance, crucial for guiding the rational design of economical  $\text{In}_2\text{O}_3$ -based catalysts. To this end, the present study aims to go beyond previous work considering just the effect of Co and systematically investigating the doping by the complete series of first-row transition metal dopants. By means of suitable density functional theory (DFT) based calculations, a series of properties such as the preferred doping site, the doping stability, the dopant Bader charge, and the effect on the density of states (DOS) are systematically evaluated. The outcome of this comprehensive investigation provides a deeper understanding of the role of dopants in modulating  $\text{In}_2\text{O}_3$ -based catalytic performance, while offers a valuable guidance

View Article Online  
DOI: 10.1039/C9CP04556H

for the rational design of efficient and economically viable catalysts for CO<sub>2</sub> hydrogenation to methanol. Simultaneously, DFT-based first-principles calculations serve as a powerful complement to experimental studies, providing atomic-level insights into structure–property relationships that are difficult to capture experimentally, thereby guiding the rational design of catalysts in materials science.

## 2. Computational details

All results reported in the present work have been extracted from DFT based calculations carried out using periodic models optimized by the Vienna *ab initio* simulation package (VASP).<sup>31,32</sup> The total energy and concomitant electronic structure was obtained using the Perdew–Burke–Ernzerhof (PBE)<sup>33</sup> exchange-correlation functional within the generalized gradient approximation (GGA), which has been shown in previous studies to reliably describe the structural and bonding energy characteristics of In<sub>2</sub>O<sub>3</sub> systems.<sup>29,34</sup> Here it is worth pointing out that it is well known that GGA functionals tend to underestimate the bandgap as predicted from the band structure.<sup>35</sup> This shortcoming can be overcome by using more sophisticated hybrid functionals introducing a fraction of non-local Fock exchange,<sup>35–37</sup> such as Heyd–Scuseria–Ernzerhof functional (HSE06). However, this significantly increases the computational cost, especially for large unit cells and a plane-wave basis set as used in this work. Moreover, the amount of Fock exchange appears to be rather material dependent,<sup>38</sup> which confers a semiempirical flavor to this approach. For a screening-oriented study, relative energy trends are more important than absolute values. Single-point calculations with the HSE06 functional based on PBE-optimized structures were performed on randomly selected dopants (Cu, Zn, Cr, and Sc), the results show that despite differences in absolute formation energies, the relative energy trends are completely consistent, as shown in Figure S1 in Supporting Information (SI). Using PBE is therefore a reasonable choice for this study. Thus, PBE functional can be regarded as suitable for this study.

A possible alternative is to make use of the include the so-called Hubbard *U* term correction term (*i.e.*, the PBE+*U* method),<sup>29,39</sup> which, nonetheless, implies a semiempirical approach as well. In this work, we uniformly adopt the PBE method (without *U*) for all calculations. This choice is justified because this study focuses on the trends in the impact of

different transition metal doping on thermodynamic stability and related electronic properties, rather than on the precise band structure or local magnetic moments, and, on the other hand, the choice of  $U$  values varies widely across different transition metals and literature sources, which could introduce artifact, systematic errors and hamper the possibility to carry out a sound comparison since, *de facto*, each systems would be treated with a different method. Finally, the previous work for Co-doped  $\text{In}_2\text{O}_3$ <sup>29</sup> has shown that PBE calculations qualitatively reproduce the main electronic structure features of this system, which is sufficient for the present purposes aimed at disclosing trends in  $\text{In}_2\text{O}_3$  doped by 3d transition metals rather than scrutinizing the precise electronic details of each system. Besides, PBE is more computationally efficient and, hence, a suitable reasonable choice for large-scale screening.

The valence electron density is expanded in a plane wave basis set, with a kinetic energy cutoff of 415 eV, and the interaction between core electrons and valence electrons is accounted for through the projector augmented wave (PAW) method.<sup>40,41</sup> The convergence threshold for the electronic self-consistency process is set to  $10^{-5}$  eV, and structural optimization is continued until the residual forces on all atoms are less than 0.01 eV/Å. For Brillouin zone integration, a  $3\times 3\times 3$  Monkhorst-Pack  $k$ -point grid centered at the  $\Gamma$  point is used. To account for long-range van der Waals interactions, the dispersion was accounted for in all calculations by means of the original D3 method with zero damping proposed by Grimme *et al.*<sup>42</sup> In addition, Gaussian smearing was employed for total energy and density of states (DOS) calculations to ensure accurate energy convergence and smooth DOS curves. Considering that all dopants involve open shells, all calculations were carried out including spin polarization.

Phonon calculations were also performed to evaluate the dynamic stability of the doped  $\text{In}_2\text{O}_3$  systems. The structures were further optimized before the phonon calculations, with a stricter electronic convergence criterion of  $1\times 10^{-8}$  eV and force on all atoms less than 0.001 eV/Å. The phonon spectra were obtained using the finite-displacement method as implemented in the PHONOPY package.<sup>43</sup>

The most stable form of the  $\text{In}_2\text{O}_3$  bulk structure used in this study is the body-centered cubic (*bcc*) bixbyite<sup>44,45</sup> crystal structure, composed of 80 atoms (see Figure 1). There are 48 oxygen atoms and two types of In atoms in different local environments, labeled as  $\text{In}_1$  and  $\text{In}_2$ ,

with 8 In<sub>1</sub> atoms and 24 In<sub>2</sub> atoms.

View Article Online  
DOI: 10.1039/D5CP04556H

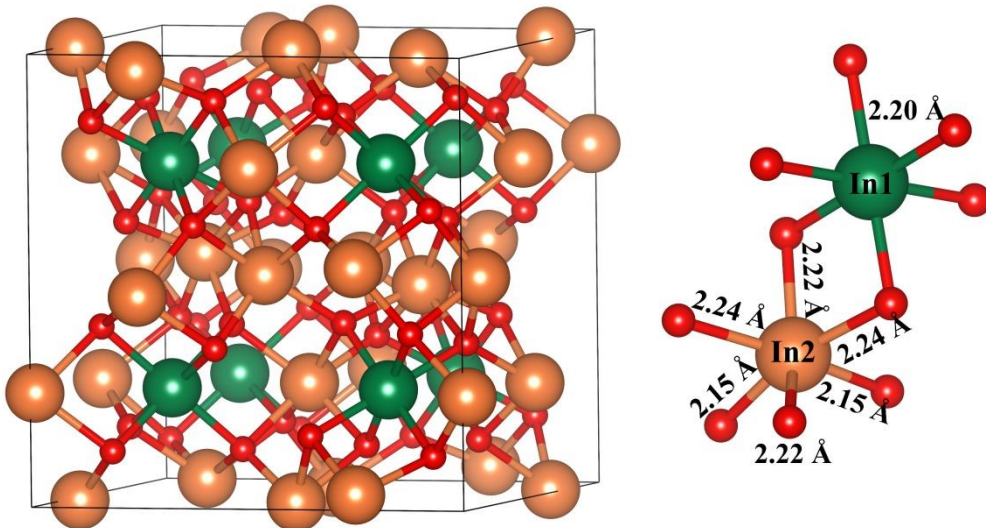


**Figure 1.** The most stable crystal structure of *bcc*  $\text{In}_2\text{O}_3$ , consisting of 80 atoms with 32 In and 48 O atoms (left). The 32 In atoms are further classified into 8 In<sub>1</sub> and 24 In<sub>2</sub> atoms (right), represented by green and orange spheres respectively, while oxygen atom is shown as red spheres.

To evaluate the stability of different neutral metal atoms doped into the  $\text{In}_2\text{O}_3$  lattice, we define the formation energy,  $\Delta E_f$ , of the doped system, as:

$$\Delta E_f = E_{\text{In}_2\text{O}_3+\text{M}} + E_{\text{In}} - E_{\text{In}_2\text{O}_3} - E_{\text{M}} \quad (1),$$

where  $E_{\text{In}_2\text{O}_3+\text{M}}$  is the total energy of the metal doped- $\text{In}_2\text{O}_3$  lattice with the M atoms substituting an In atom on the lattice,  $E_{\text{In}_2\text{O}_3}$  is the total energy of the  $\text{In}_2\text{O}_3$  cell,  $E_{\text{In}}$  is the energy of a single In atom, referenced to the energy of bulk In, and  $E_{\text{M}}$  is the energy of a doping metal atom, also referenced to the energy of M bulk.

In addition, we also considered the cohesive energy,  $E_{\text{coh}}$ , to evaluate the stability of the doped systems, as follows:

$$E_{\text{coh}} = \frac{(N_M \cdot E_M + N_{\text{In}} \cdot E_{\text{In}} + N_O \cdot E_O) - E_{\text{In}_2\text{O}_3+\text{M}}}{N_{\text{total}}} \quad (2),$$

here,  $N_M$ ,  $N_{\text{In}}$ , and  $N_O$  represent the numbers of doped metal, In, and O atoms in the doped supercell, respectively.  $E_M$ ,  $E_{\text{In}}$ , and  $E_O$  denote the energies of isolated doped metal, In, and O atoms.  $E_{\text{In}_2\text{O}_3+\text{M}}$  is the total energy of the metal-doped  $\text{In}_2\text{O}_3$  lattice with the M atom

substituting an In atom, similar to Eq. 1.  $N_{\text{total}}$  is the total number of atoms in the studied system. To clearly show the effect of the dopant on the cohesive energy, the difference between the values for the undoped and doped systems,  $\Delta E_{\text{coh}}$ , is also considered.

We note here that using the bulk reference avoids the problems related to the use of a single Slater determinant to approach the open shell multiple ground state of atoms and, also, the use of a broken symmetry solution and the incorrect occupancy of predicted by PBE for some atoms.<sup>46</sup> Note also that the energy formation with respect to the gas phase atoms can be readily obtained from the cohesive energy of the metal taken from calculations or from experiment (see *e.g.* Refs. 47 and 48). With this definition, a negative value of  $\Delta E_f$  indicates that doping is energetically favorable. Finally, to understand the main effects of doping on chemical features we rely on Bader charges and DOS analysis.

### 3. Results and discussion

#### 3.1. Doping sites preference and electronic properties

As above stated, in bulk  $\text{In}_2\text{O}_3$  bixbyite phase there are two different In sites; In1 and In2. The O atoms coordination environment around In1 differs from that around In2 (*cf.* Figure 1), which may lead to a preference for the doping transition metal (TM) atoms to occupy different positions. The optimized lattice parameters are consistent with previously reported values with deviations of at most 0.040 Å, and also a good agreement with experimental data derived from XRD measurements, with 0.063 Å.<sup>29</sup> Here we first systematically investigated the stability of the first-row TMs (TM = Sc, Ti, V, Cr, Mn, Fe, Co, Ni, Cu, Zn) when substituting the In1 and In2 sites, which ultimately defines the subsequent doping effects. The  $\Delta E_f$  is a key indicator of the thermodynamic stability of the doping process, and the gained results are shown in Table 1, revealing that most TMs (*i.e.* Sc, Ti, V, Mn, Ni, and Zn) preferentially occupy the In2 site, while Cr, Co, Fe, and Cu tend to be favored on the In1 site —consistent with previous finding for Co.<sup>29</sup>

This site preference is likely to be governed by the interplay between the electronic configuration of dopant and the local symmetry of the host sites. The In1 site, with six equivalents In–O bonds, provides a highly symmetric octahedral environment that may better accommodate metals with an electron configuration with single  $s$  orbital occupancy and half-

filled or fully filled *d*-shells, such as Cr and Cu with Ar[4s<sup>1</sup>3d<sup>5</sup>] and Ar[4s<sup>1</sup>3d<sup>10</sup>]<sup>10</sup> electron configuration, respectively, as well as metals with a relatively high number of *d*-electrons such as Co and Fe with Ar[4s<sup>2</sup>3d<sup>7</sup>] and Ar[4s<sup>2</sup>3d<sup>6</sup>] electron configuration, respectively.

In contrast, the lower symmetry and distorted site of In2 site may allow more structural flexibility, stabilizing other dopants. For instance, Mn and Zn with an electron configuration with fully filled 4s orbitals may likely prefer In2 site. This observation suggests that, in addition to the occupancy of the *d* orbitals, the occupancy of the *s* orbitals may also influence the doping site in In<sub>2</sub>O<sub>3</sub>. Nevertheless, one must note that the electron configuration of the dopant in the host crystal is for sure different from that in vacuum as evidenced by the Bader charges in Table 1. Hence, the reasoning arguments above have to be taken with a grain of salt, and just as a first qualitative interpretation, because the doping site preference for first-row transition metal dopants in In<sub>2</sub>O<sub>3</sub> is a complex process involving multiple factors going from the electronic structure of the metal, to the symmetry and geometric configuration of the doping site.

**Table 1.** Ground state electronic configuration of the isolated atom, preferred doping site (In1/In2),  $\Delta E_f$  (eV),  $\Delta E_{coh}$  (eV), Bader charge,  $Q$  (e), *d*-band center,  $\varepsilon_d$ , in eV, local magnetic moment ( $\mu_{local}$ ,  $\mu_B$ ) and total magnetic moment ( $\mu_{total}$ ,  $\mu_B$ ) of the first-row transition metal doped In<sub>2</sub>O<sub>3</sub> systems.

M	Electronic configuration	Doping site	$\Delta E_f$	$\Delta E_{coh}$	$Q$	$\varepsilon_d$	$\mu_{local}$	$\mu_{total}$
<b>Sc</b>	[Ar]4s <sup>2</sup> 3d <sup>1</sup>	In2	-6.72	0.01	2.04	5.51	0	0
<b>Ti</b>	[Ar]4s <sup>2</sup> 3d <sup>2</sup>	In2	-5.59	0.03	2.17	0.31	0	0
<b>V</b>	[Ar]4s <sup>2</sup> 3d <sup>3</sup>	In2	-3.15	-0.03	1.80	1.01	1.40	1.38
<b>Cr</b>	[Ar]4s <sup>1</sup> 3d <sup>5</sup>	In1	-2.64	0.01	1.76	0.11	2.75	2.75
<b>Mn</b>	[Ar]4s <sup>2</sup> 3d <sup>5</sup>	In2	-1.63	0.02	1.62	-0.40	3.58	3.71
<b>Fe</b>	[Ar]4s <sup>2</sup> 3d <sup>6</sup>	In1	0.28	0.00	1.45	-0.41	1.26	1.23
<b>Co</b>	[Ar]4s <sup>2</sup> 3d <sup>7</sup>	In1	0.32	0.08	1.30	-0.34	0	0
<b>Ni</b>	[Ar]4s <sup>2</sup> 3d <sup>8</sup>	In2	1.15	0.09	1.25	-1.22	0.74	0.95
<b>Cu</b>	[Ar]4s <sup>1</sup> 3d <sup>10</sup>	In1	1.66	0.06	1.27	-2.84	0.83	1.82

Zn	[Ar]4s <sup>2</sup> 3d <sup>10</sup>	In2	0.26	-0.04	1.33	-4.19	0.02	0.02
----	--------------------------------------	-----	------	-------	------	-------	------	------

### 3.2. Stability and Bader charge analysis

The  $\Delta E_f$  shown in Table 1 and Figure 2 reveal that  $\Delta E_f$  increases steadily from Sc to Zn, indicating a gradual decrease in the easiness of doping across the series. For Sc to Mn, the formation energies are negative (-6.72, -5.59, -3.15, -2.64 and -1.63 eV for Sc, Ti, V, Cr, and Mn, respectively), decreasing in magnitude with increasing the atomic number. This supports that doping with this early transition metal (Sc, Ti, V, and Cr) is thermodynamically favorable, while Mn marks the transition towards the energetically unfavorable late transition metals. In contrast, the formation energies from Fe to Zn are all positive (0.28, 0.32, 1.15, 1.66, and 0.26 eV for Fe, Co, Ni, Cu, and Zn, respectively), indicating that these doped systems have limited thermodynamic stability.

Similarly, the local site symmetry and geometry of the  $\text{In}_2\text{O}_3$  lattice may also influence the dopant formation energies. Metals that prefer the higher-symmetry In1 site (Fe, Co, Cu) generally exhibit higher  $\Delta E_f$  than those favoring the lower-symmetry In2 site (Sc, Ti, V, Mn, Zn), supporting the interpretation that site symmetry and local geometry significantly influence the doping atom stability.

Notably, Zn shows a relatively low formation energy (0.26 eV) compared to those of elements ranging from Fe to Cu, deviating from the general increasing trend. This anomaly may be attributed to the unique fully filled  $4s^23d^{10}$  electronic configuration of Zn, which may result in different charge transfer behavior or bonding with oxygen atoms when interacting with the  $\text{In}_2\text{O}_3$  lattice. Beyond the influence of electronic configurations, dispersion interactions also contribute to the dopant formation energies. Without including dispersion through the DFT-D3 method, Fe (2.57 eV) was predicted as the most stable, followed by Co (2.63 eV) and Zn (2.70 eV). However, the  $3d^{10}$  closed-shell configuration of Zn makes it more responsive to dispersion interactions, resulting in a stability gain of -2.44 eV compared to the open-shell Fe (-2.29 eV) and Co (-2.31 eV), as shown in Figure S2 in SI. This small difference in correction was sufficient to reverse their stability order, leading to the ordering Zn < Fe < Co.

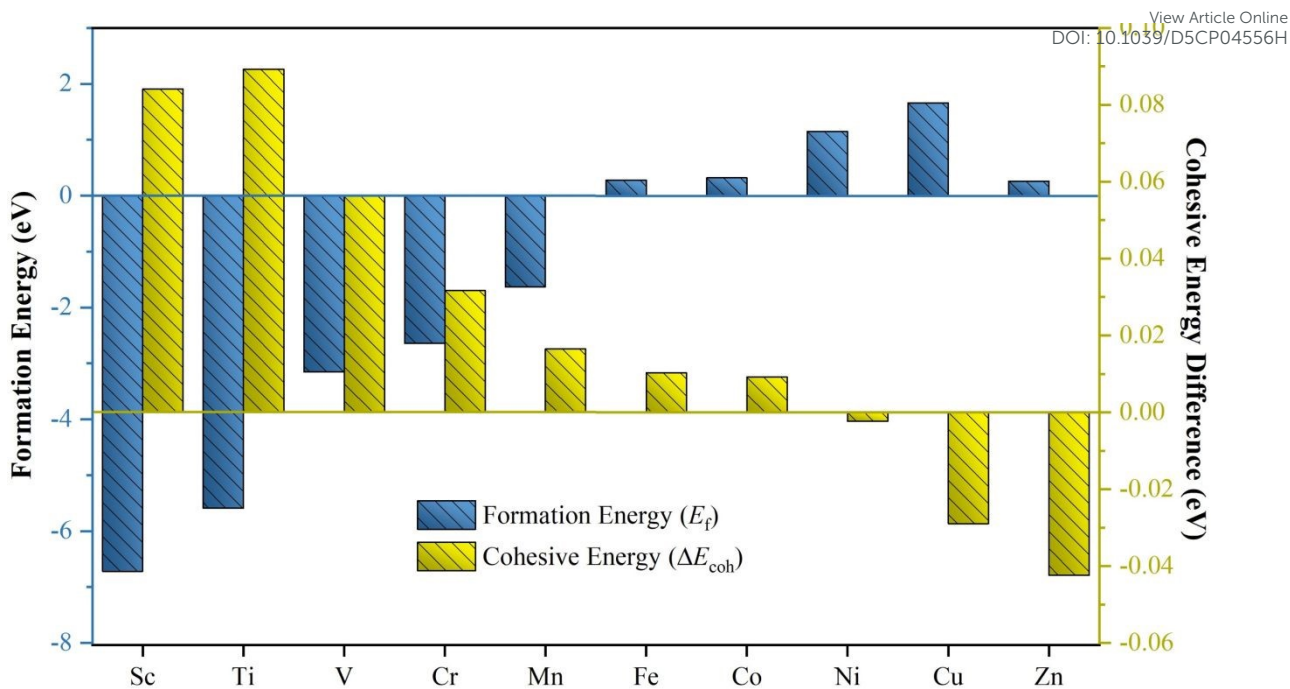


**Figure 2.** Formation energies ( $E_f$ ) and cohesive energies ( $E_{coh}$ ) of  $\text{In}_2\text{O}_3$  doped with first-row 3d TMs.  $E_f$  and  $E_{coh}$  correspond to the blue and yellow squares, respectively.

In addition to the  $\Delta E_f$ , which reflects the feasibility of doping, we also analyzed the cohesive energy,  $E_{coh}$ , to evaluate the structural stability of the doped systems. As shown in Table 1 and Figure 2, all doped systems exhibit high cohesive energies within a narrow range (4.68 eV/atom for Zn to 4.81 eV/atom for Ti), indicating that they are all robust and structurally stable. Furthermore, since Sc-doped  $\text{In}_2\text{O}_3$  was identified as the most thermodynamically stable system ( $\Delta E_f = -6.72$  eV), we further assessed its dynamic stability through specifically including phonon calculations. The obtained phonon band structure shows no imaginary frequencies throughout the entire Brillouin zone, as displayed in the left panel of Figure 3, which is consistent with the phonon density of states (DOS) shown in the right panel. The corresponding reciprocal space and the high-symmetry  $k$ -paths of  $\Gamma$ —X—Y— $\Gamma$ —Z—R— $\Gamma$ —T—U— $\Gamma$ —V are shown in Figure S3 of the SI. These results confirm the dynamic stability of the Sc-doped  $\text{In}_2\text{O}_3$  system. Meanwhile, the phonon-derived thermodynamic properties of the system were also calculated (Figure S4 of the SI). As the temperature increases, the free energy decreases while the entropy increases, consistent with thermodynamic principles. In addition,

the heat capacity ( $C_v$ ) at constant volume was calculated using the well-known relation (Eq. 3) implemented in PHONOPY program,<sup>43</sup>

$$C_v = R \int_0^{\omega_{\max}} \left( \frac{\hbar\omega}{k_B T} \right)^2 \frac{\frac{\hbar\omega}{e^{\frac{\hbar\omega}{k_B T}} - 1}}{g(\omega)} d\omega \quad (3)$$

where  $g$  is the phonon DOS,  $\omega$  denotes the vibrational frequency,  $R$ ,  $k_B$ , and  $T$  stand for the gas constant, Boltzmann constant, and temperature, respectively. The results showed that the  $C_v$  rises with temperature and becomes nearly unchanged above about 400 K, showing thermodynamically reasonable behavior.

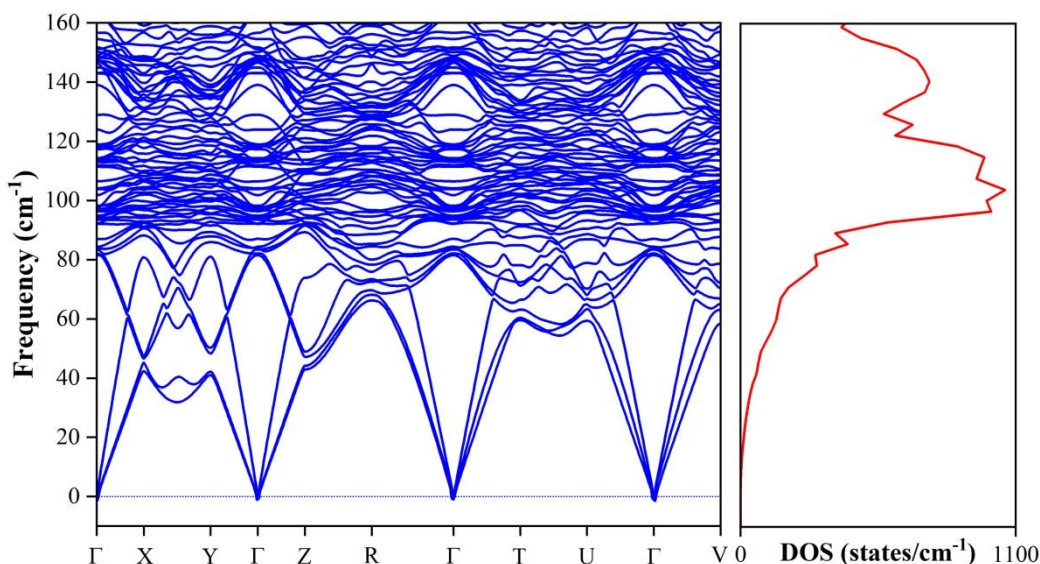


**Figure 3.** (a) Phonon band structure of Sc-doped  $\text{In}_2\text{O}_3$  along high-symmetry paths of the Brillouin zone, and (b) its corresponding phonon density of states (DOS).

In addition to thermodynamic and dynamic stability analyses, we performed a systematic spin-polarization analysis to investigate the intrinsic electronic structure and spin polarization effects of the TM dopants. The magnetic moments,  $\mu_B$ , are characterized by local magnetic moments ( $\mu_{\text{local}}$ ) for doped metal atom, and the total magnetic moment ( $\mu_{\text{total}}$ ) for the entire unit cell, with results summarized in Table 1. The results show that the magnetic behavior strongly depends on the dopant. Sc, Ti, Co, and Zn converged to a non-magnetic ground state ( $\mu_{\text{total}} \approx 0$

$\mu_B$ ), which is physically sound, as Sc ( $3d^1$ ) and Ti ( $3d^2$ ) readily lose their few d-electrons to the surrounding oxygen atoms, allowing them to achieve a stable, non-magnetic  $d^0$  ionic state. In contrast, Zn possesses a stable  $3d^{10}$  closed-shell configuration, which is difficult to lose these paired d-electrons, also resulting in no magnetic moment. Whereas Co ( $3d^7$ ) is a special case, adopting a stable low-spin state in In1 site, which leads to a zero net moment. In contrast, V, Cr, Mn, Fe, Ni, and Cu all exhibited magnetic ground states due to unpaired d-electrons, with strongly localized magnetic moments close to their total moments ( $\mu_{\text{local}} \approx \mu_{\text{total}}$ ). However, for systems like Cu, the total moment ( $\mu_{\text{total}} \approx 1.82 \mu_B$ ) is significantly larger than the local moment ( $\mu_{\text{local}} \approx 0.83 \mu_B$ ), indicating a strong spin polarization of the surrounding O atoms in the  $\text{In}_2\text{O}_3$  lattice.

Finally, to further understand the behavior of metal dopants in the  $\text{In}_2\text{O}_3$  lattice, we analyzed in detail the trends of the Bader charges reported in Table 1. In all cases, there is clear trend to transfer electrons from the metal atom to the host oxide, so that the dopant gets positively charged, as expected from the rather high ionic character of the chemical bonding in  $\text{In}_2\text{O}_3$ .<sup>49</sup> Nevertheless, results in Table 1 indicate that the doped metal atoms exhibit markedly different charges. For instance, Ti shows the largest  $+2.17 e$  charge, forming strong coulombic interactions with the surrounding O atoms of the  $\text{In}_2\text{O}_3$  lattice, in line with the strong ionic character of the host crystal. Nevertheless, rather large differences are encountered along the 3d series with dopants such as Ni and Cu being less charged;  $+1.25$  and  $+1.27 e$ , respectively, likely due to a trend to keep the d shell almost filled.

To better understand these trends, the correlation between the formation energies and the Bader charges of the doped metal atoms was analyzed in Figure 4, revealing a strong linear relationship with a regression coefficient of  $R = 0.974$ . This indicates that the amount of charge transferred from the dopant atom plays a key, determining role. Thus, a larger electron transfer is directly associated with a lower (more negative) formation energy, implying an enhanced thermodynamic stability. In contrast, those dopant metal atoms that transfer fewer electrons tend to exhibit higher (more positive) formation energies, indicating a reduced stability of the doping process.

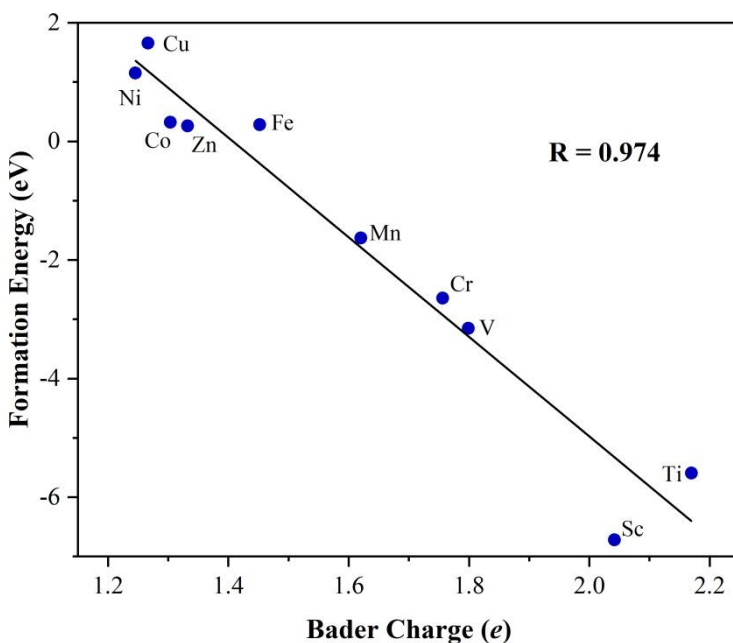


**Figure 4.** Linear correlation of the 3d TM doped  $\text{In}_2\text{O}_3$  systems formation energies *vs.* the calculated Bader charges.

### 3.3. Electronic structure analysis

A better picture of the electronic structure changes induced by dopant metal atoms can be gained from the DOS analysis, specially when projected on the elementary components, as done in Figure 5. These plots illustrate the distribution of the electronic states near the Fermi level,  $E_F$ , as well as the valence and conduction band regions. Firstly, the projected DOS (PDOS) shows O dominancy in the valence band (from *ca.* -6 to 0 eV with respect  $E_F$ ), consistent with its high electronegativity and electron affinity, reflecting its role as the primary bonding element. In more detail, the contributions near  $E_F$  arise from the hybridization of O 2p orbitals with In orbitals. Furthermore, In 5s and 5p electrons contribute significantly to the valence band, where a strong hybridization between In and O atomic orbitals agrees with the formation of In–O bonds with partial covalent character, as discussed in a previous work.<sup>49</sup> However, near  $E_F$ , the hybridization becomes weaker as In is partially oxidized with a concomitant depletion of its 5s/5p orbitals. In the conduction band region, a higher degree of hybridization is observed between the 5s/5p orbitals of indium and the 2p orbitals of oxygen.



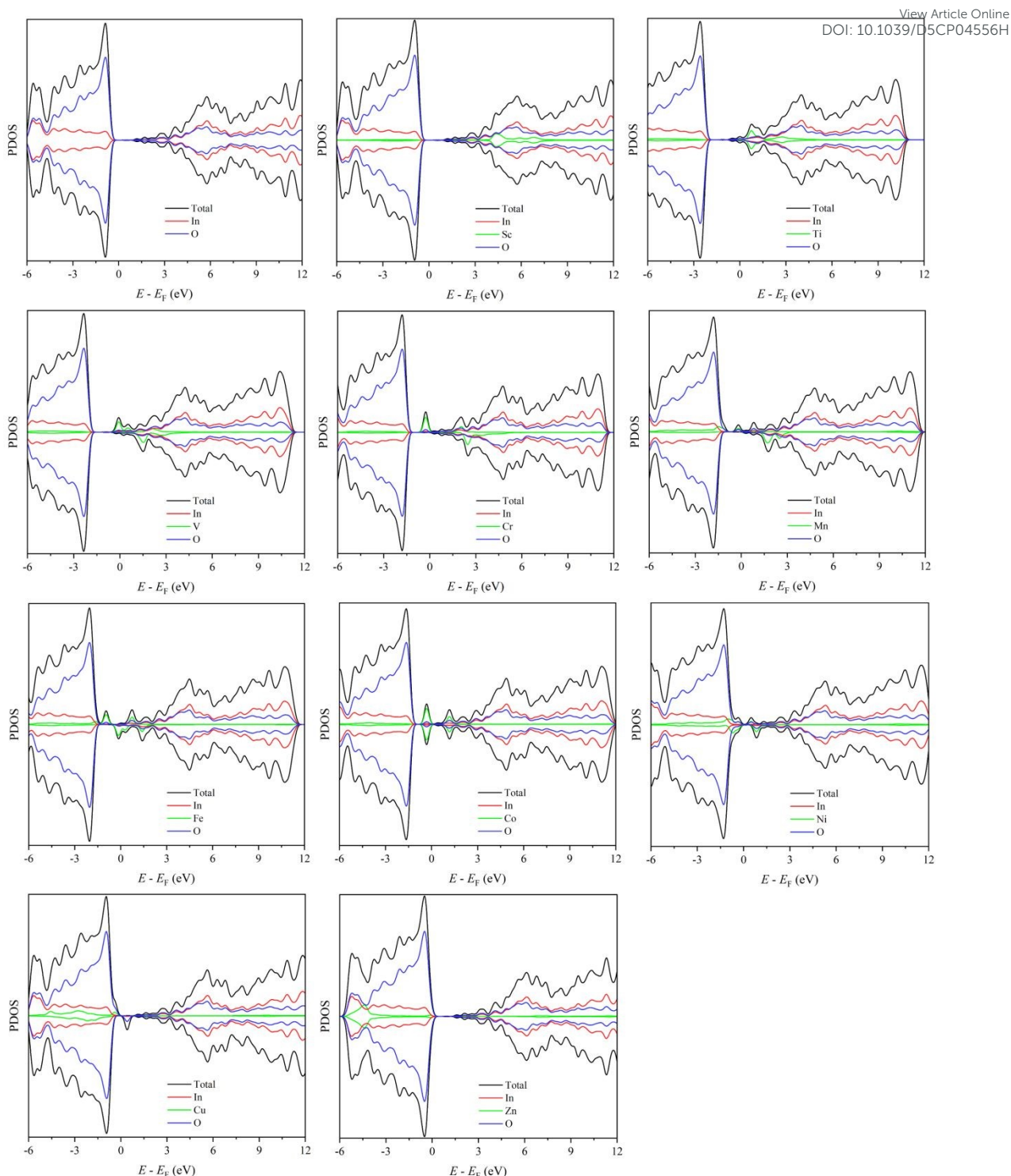


**Figure 5.** Total and PDOS of the first-row transition metals-doped  $\text{In}_2\text{O}_3$  systems. All energies are referred to Fermi energy,  $E_F$ , defined here as the maximum of the valence band.

Regarding the  $3d$  orbital electron distributions of the TM dopants, there are significant differences, with complex peak features near  $E_F$ , reflecting the splitting of  $d$  electron energy levels and their interaction with the coordination environment. Taking the early transition metal



Sc as an example, the ground-state electron configuration for the isolated atoms is  $1s^2 3d^1$ . Due to the presence of only one electron in the  $3d$  orbital, Sc doping tends to donate  $4s$  and  $3d$  electron density, resulting in a lower density of state near  $E_F$ , with peaks primarily appearing in the conduction band region ( $E - E_F \approx 4.5$  eV).

In contrast, Ti, V, and Cr, although being also early TMs, have more  $3d$  electrons with a concomitant pronounced  $3d$  states density near  $E_F$ , suggesting more active involvement of  $3d$  electron states in charge transfer. For the late transition metals Fe and Co, their  $3d$  orbital energy levels make a significant contribution near  $E_F$ , characterized by broad and overlapping peaks that reflect strong hybridization between valence and conduction band edges. By contrast, Mn and Ni show relatively weaker  $3d$  states contributions around  $E_F$ , which may be attributed to differences in their distinct electron configurations and specific orbital hybridization within the doped systems. For Mn, with its  $3d^5$  high-spin configuration, the strong electron-electron repulsion leads to  $d$ -electron localization, which is consistent with the high local magnetic moment ( $3.58 \mu_B$ ) showed in Table 1. This localization may limit the orbital hybridization with neighboring atoms, resulting in a reduced  $d$  state density near  $E_F$ .<sup>50,51</sup> On the other hand, Ni, with its  $3d^8$  configuration, experiences a quite filled  $3d$  shell, which promotes electron localization.<sup>52</sup> Finally, the  $3d$  orbitals of the late transition metals Cu and Zn exhibit typical characteristics near  $E_F$  arising from their nearly fully  $3d$  shell, all mainly distributed in the valence band region (below  $E_F$ ), with almost no contribution near  $E_F$ . This absence of  $3d$  orbital contribution near the Fermi level is a significant feature of the electronic structure of late transition metals, especially Zn.

The  $d$  band center,<sup>53</sup>  $\varepsilon_d$ , calculated following the commonly accepted approach,<sup>54</sup> is usually employed as a descriptor in catalysis, especially for metallic surfaces<sup>55</sup> where this band is broad enough. Indeed, this descriptor is almost independent of the density functional used,<sup>56</sup> which makes it especially interesting for comparing different studies. For the present systems with a very low dopant concentration, the  $d$  band is quite narrow. Yet, its position relative to  $E_F$  may offer additional information of interest in catalysis, and the position is precisely provided by the  $d$  band center. Therefore, the  $d$  band center of the TM dopants in  $\text{In}_2\text{O}_3$  was computed, and values listed in Table 1.

A clear correlation between  $\varepsilon_d$  values and the corresponding  $\Delta E_f$  emerges as shown in Figure 6. In general, dopants with higher  $d$  band center values tend to exhibit lower (more negative) formation energies. For instance, Sc exhibits a  $\varepsilon_d$  value of 5.51 eV and a formation energy of -6.72 eV, while Zn exhibits a  $\varepsilon_d$  of -4.19 eV and a formation energy of 0.26 eV. Nevertheless, the correlation between the  $d$  band center and formation energy is only qualitative, with an  $R = 0.803$ , but, in any case, indicates that the  $\varepsilon_d$  also may serve as a moderate descriptor for assessing the favorability of the doping process in  $\text{In}_2\text{O}_3$ .

View Article Online  
DOI: 10.1039/D5CP04556H

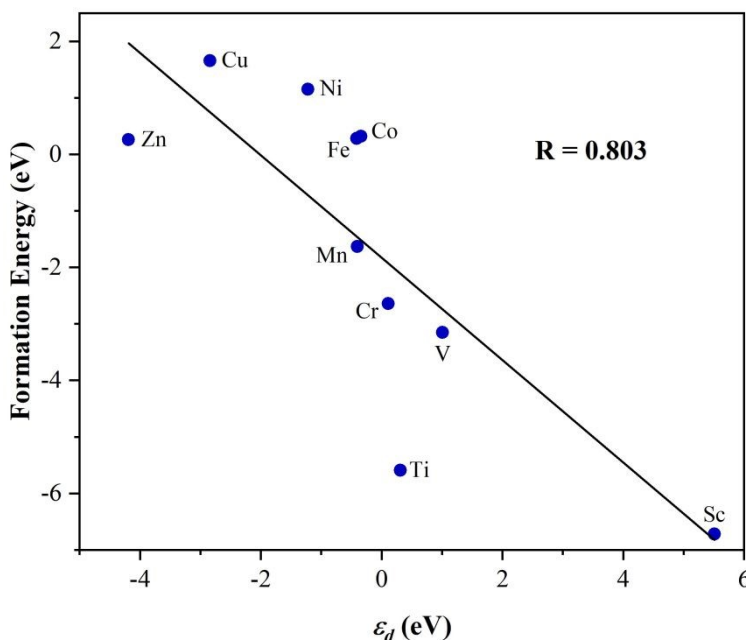


**Figure 6.** Linear correlation of the 3d TM doped  $\text{In}_2\text{O}_3$  systems formation energies *vs.* the TM  $\varepsilon_d$  values.

The distinct PDOS features and  $\varepsilon_d$  values among different metals clearly reflect variations in hybridization characteristics and electronic structure. These results offer valuable insights for designing and selecting TM dopants with targeted stability and electronic properties.

#### 4. Conclusions

Based on DFT, the present study systematically investigates the properties of  $\text{In}_2\text{O}_3$  doped with the first-row TMs, with a focus put on the structural stability and main electronic structure features. The results demonstrate that the electronic configurations of the dopants strongly influence their preferred doping sites, stability, charge transfer behavior, and PDOS features of the systems. Early TMs (such as Sc, Ti, V, Cr) exhibit a pronounced thermodynamic stability,

with generally negative formation energies, indicating a favorable doping. These metals would tend to substitute the relatively lower symmetry In<sub>2</sub> site, forming more stable coordination environments. In contrast, formation energies for metal dopants from Fe to Zn gradually increase along the 3d series, with Ni and Cu exhibiting particularly high values, indicating more unfavorable doping processes.

Bader charge analysis further revealed that a significant charge transfer from the dopant metal atoms to the In<sub>2</sub>O<sub>3</sub> lattice, with a strong linear correlation between the Bader charge and formation energy, suggesting that the metal electron donating ability is a key factor governing the thermodynamic stability of the doped system. The PDOS analysis reveals that the *d* state density near  $E_F$  is strongly influenced by the 3d occupancy. The  $\varepsilon_d$  of the metal has been estimated and found to exhibit a moderate linear trend with the formation energy indicating that this descriptor may be useful to assess the stability of In<sub>2</sub>O<sub>3</sub> systems doped with TMs, at least, in a qualitative fashion. Metals with higher  $\varepsilon_d$ , such as Sc, Ti, V and Cr, tend to form more stable systems, whereas those with lower  $\varepsilon_d$ , like Cu and Zn, are associated with higher formation energies.

This study systematically reveals the intrinsic relationships among structure, stability, and electronic properties of first-row transition metal-doped In<sub>2</sub>O<sub>3</sub> systems. Specially, dopants such as Ti, V, and Cr, characterized by a high stability, strong electron transfer ability, and prominent *d* band states contribution near  $E_F$ , are expected to facilitate further optimization of In<sub>2</sub>O<sub>3</sub>-based catalysts. These findings deepen the understanding of doping regulation mechanisms and offer theoretical guidance for designing efficient CO<sub>2</sub> hydrogenation catalysts.

## Acknowledgements

[View Article Online](#)  
DOI: 10.1039/D5CP04556H

The present work received financial support from the Spanish *Ministerio de Ciencia e Innovación* and *Agencia Estatal de Investigación* (AEI) MCIN/AEI/10.13039/501100011033 and, as appropriate, by “European Union Next Generation EU/PRTR”, through grants TED2021-129506B-C22, PID2021-126076NB-I00, PID2024-159906NB-I00, *la Unidad de Excelencia María de Maeztu* CEX2021-001202-M granted to the ITQCUB and, in part, from *Generalitat de Catalunya* 2021SGR00079 grant. The *Red Española de Supercomputación* (RES projects QHS-2024-1-0001, QHS-2024-2-0014, and QHS-2024-3-0008) and *Consorci de Serveis Universitaris de Catalunya* (CSUC) are also acknowledged for the generous computational resources. F.V. is thankful for the ICREA Academia Award 2023 Ref. Ac2216561

## References

1. F. J. Wentz, L. Ricciardulli, K. Hilburn and C. Mears, *Science*, 2007, **317**, 233–235.
2. C. Tebaldi, R. Ranasinghe, M. Voudoukas, D. J. Rasmussen, B. Vega-Westhoff, E. Kirezci, R. E. Kopp, R. Srivastava and L. Mentaschi, *Nat. Clim. Change.*, 2021, **11**, 746–751.
3. C. Costentin, M. Robert and J.-M. Savéant, *Chem. Soc. Rev.* 2013, **42**, 2423–2436.
4. L. Meng, L.-K. Yan, F. Viñes and F. Illas, *J. Mater. Chem. A*, 2024, **12**, 7856–7874.
5. M. D. Garba, M. Usman, S. Khan, F. Shehzad, A. Galadima, M. F. Ehsan, A. S. Ghanem and M. Humayun, *J. Environ. Chem. Eng.*, 2021, **9**, 104756.
6. A. Modak, P. Bhanja, S. Dutta, B. Chowdhury and A. Bhaumik, *Green Chem.*, 2020, **22**, 4002–4033.
7. O. Awogbemi and D. A. Desai, *Discov. Nano*, 2025, **20**, 29.
8. I. I. Maor, S. Heyte, O. Elishav, M. Mann-Lahav, J. Thuriot-Roukos, S. Paul and G. S. Grader, *Nanomaterials.*, 2023, **13**, 635.
9. N. Onishi and Y. Himeda, *Acc. Chem. Res.*, 2024, **57**, 2816–2825.
10. X. Li, Q. Cheng, Y. Zhang, Y. Liu, Y. Pan, D. Zhao, S. Xiong, W. Liu, X. Jiang, J. Yan, X. Duan, Y. Tian and X. Li, *Angew. Chem. Int. Ed.*, 2025, **64**, e202424435.
11. S. Kar, R. Sen, A. Goeppert and G. K. S. Prakash, *J. Am. Chem. Soc.*, 2018, **140**, 1580–1583
12. H. Zada, J. Yu and J. Sun, *ChemSusChem*, 2025, **18**, e202401846.
13. H. H. Wong, M. Sun, T. Wu, C. H. Chan, L. Lu, Q. Lu, B. Chen and B. Huang, *eScience*, 2024, **4**, 100140.
14. U. J. Etim, C. Zhang and Z. Zhong, *Nanomaterials*, 2021, **11**, 3265.
15. T. S. Bui, E. C. Lovell, R. Daiyan and R. Amal, *Adv. Mater.*, 2023, **35**, 2205814.
16. G. Pacchioni, *ChemPhysChem* 2003, **4**, 1041–1047.
17. T. Pinheiro Araújo, C. Mondelli, M. Agrachev, T. Zou, P. O. Willi, K. M. Engel, R. N. Grass, W. J. Stark, O. V. Safonova, G. Jeschke, S. Mitchell and J. Pérez-Ramírez, *Nat. Commun.*, 2022, **13**, 5610.
18. L. Liu, B. Mezari, N. Kosinov and E. J. M. Hensen, *ACS Catal.*, 2023, **13**, 15730–15745.

19. F. Cannizzaro, E. J. M. Hensen and I. A. W. Filot, *ACS Catal.*, 2023, **13**, 1875–1892.

20. J. Wang, G. Zhang, J. Zhu, X. Zhang, F. Ding, A. Zhang, X. Guo and C. Song, *ACS Catal.*, 2021, **11**, 1406–1423.

21. S. Dang, B. Qin, Y. Yang, H. Wang, J. Cai, Y. Han, S. Li, P. Gao and Y. Sun, *Sci. Adv.*, 2020, **6**, eaaz2060.

22. D. Cai, Y. Cai, K. B. Tan and G. Zhan, *Materials*, 2023, **16**, 2803.

23. Z. Meng, X. Sun, Y. Tang, B. Yan, Z. Zhao and B. Li, *ChemCatChem*, 2025, **17**, e202401298.

24. Z. Ren, B. Li, Y. Wu, H. Liu, F. Guo, S. Tian and J. Yang, *Chem. Eng. J.*, 2025, **507**, 160394

25. N. H. M. D. Dostagir, C. Thompson, H. Kobayashi, A. M. Karim, A. Fukuoka and A. Shrotri, *Catal. Sci. Technol.*, 2020, **10**, 8196–8202

26. Z. Liu, H. Liu, M. Li, Y. Meng, X. Wang, T. Yan, Q. Fan, S. N. Lou, W. Cui and S. Zhang, *ChemCatChem*, 2024, **16**, e202301700.

27. A. Bavykina, I. Yarulina, A. J. Al Abdulghani, L. Gevers, M. N. Hedhili, X. Miao, A. R. Galilea, A. Pustovarenko, A. Dikhtiarenko, A. Cadiau, A. Aguilar-Tapia, J.-L. Hazemann, S. M. Kozlov, S. Oud-Chikh, L. Cavallo and J. Gascon, *ACS Catal.*, 2019, **9**, 6910–6918.

28. N. Wubulikasimu, R. Shen, L. Hao, H. He, K. Li, X. Li and J. Xie, *Chem. Eng. J.*, 2024, **501**, 157397.

29. M. Voccia, S. Kapse, R. Sayago-Carro, N. Gómez-Cerezo, M. Fernández-García, A. Kubacka, F. Viñes and F. Illas, *ACS Appl. Mater. Interfaces*, 2024, **16**, 30157–30165.

30. S. Kapse, F. Viñes and F. Illas, *J. Phys. Chem.*, in press

31. G. Kresse and J. Furthmüller, *Phys. Rev. B*, 1996, **54**, 11169–11186.

32. G. Kresse and J. Furthmüller, *Comput. Mater. Sci.*, 1996, **6**, 15–50.

33. J. P. Perdew, K. Burke and M. Ernzerhof, *Phys. Rev. Lett.*, 1996, **77**, 3865–3868.

34. M. S. Frei, M. Capdevila-Cortada, R. García-Muelas, C. Mondelli, N. López, J. A. Stewart, D. Curulla Ferré and J. Pérez-Ramírez, *J. Catal.*, 2018, **361**, 313–321.

35. C. Sousa, S. Tosoni and F. Illas, *Chem. Rev.*, 2013, **113**, 4456–4495

36. J. Muscat, A. Wander and N. M. Harrison, *Chem. Phys. Lett.*, 2001, **342**, 397–401.

37. I. de P.R. Moreira, F. Illas and R. L. Martin, *Phys. Rev. B* 2002, **65**, 155102.

38. K. C. Ko, O. Lamiel-García, J. Y. Lee and F. Illas, *Phys. Chem. Chem. Phys.* 2016, **18**, 12357–12367.

39. S. L. Dudarev, G. A. Botton, S. Y. Savrasov, C. J. Humphreys and A. P. Sutton, *Phys. Rev. B*, 1998, **57**, 1505–1509.

40. P. E. Blöchl, *Phys. Rev. B*, 1994, **50**, 17953–17979.

41. G. Kresse and D. Joubert, *Phys. Rev. B*, 1999, **59**, 1758–1775.

42. S. Grimme, J. Antony, S. Ehrlich and H. Krieg, *J. Chem. Phys.* 2010, **132**, 154104.

43. A. Togo and I. Tanaka, *Scripta Mater.*, 2015, **108**, 1–5.

44. J. Ederth, P. Johnsson, G. A. Niklasson, A. Hoel, A. Hultåker, P. Heszler, C. G. Granqvist, A. R. van Doorn, M. J. Jongerius and D. Burgard, *Phys. Rev. B*, 2003, **68**, 155410.

45. G. B. González, J. B. Cohen, J. H. Hwang, T. O. Mason, J. P. Hodges and J. D. Jorgensen, *J. Appl. Phys.*, 2001, **89**, 2550–2555.

46. A. Markovits, J. C. Paniagua, N. López, C. Minot and F. Illas, *Phys. Rev. B*, 2003, **67**, 115417.

47. P. Janthon, S. M. Kozlov, F. Viñes, J. Limtrakul and F. Illas, *J. Chem. Theory Comput.* 2013, **9**, 1631–1640.

48. P. Janthon, S. Luo, S. M. Kozlov, F. Viñes, J. Limtrakul, D. G. Truhlar and F. Illas, *J. Chem. Theory Comput.*, 2014, **10**, 3832–3839.

49. S. Kapse, M. Voccia, F. Viñes and F. Illas, *J. Mol. Model.*, 2024, **30**, 161.

50. T. Paiva, G. Esirgen, R. T. Scalettar, C. Huscroft and A. K. McMahan, *Phys. Rev. B*, 2003, **68**, 195111.

51. N. U. Din, T. Jiang, S. Gholam-Mirzaei, M. Chini and V. Turkowski, *J. Phys. Condens. Matter*, 2020, **32**, 475601.

52. N. A. Dodd, Y. Cao, J. Bacsa, E. C. Towles, T. G. Gray and J. P. Sadighi, *Inorg. Chem.*, 2022, **61**, 16317–16324.

53. B. Hammer and J.K. Nørskov, *Surf. Sci.*, 1995, **343**, 211–220.

54. I. Demiroglu, Z. Y. Li, L. Piccolo and R. L. Johnston, *Catal. Sci. Technol.*, 2016, **6**, 6916–6931.

55. J. K. Nørskov, T. Bligaard, J. Rossmeisl and C.H. Christensen, *Nat. Chem.*, 2009, **1**, 37–46.
56. L. Vega, B. Martínez , F. Viñes and F. Illas, *Phys. Chem. Chem. Phys.*, 2018, **20**, 20548–20554.

# Computational Insights into the Structural and Electronic Properties of First-Row Transition Metal-Doped $\text{In}_2\text{O}_3$ Systems

Ling Meng,<sup>ab</sup> Francesc Viñes<sup>a</sup> and Francesc Illas<sup>\*a</sup>

<sup>a</sup> Departament de Ciència de Materials i Química Física & Institut de Química Teòrica i Computacional (IQT CUB), Universitat de Barcelona, c/ Martí i Franquès 1-11, 08028, Barcelona, Spain.

<sup>b</sup> State Key Laboratory of Chemical Resource Engineering, Beijing Engineering Center for Hierarchical Catalysts, College of Chemistry, Beijing University of Chemical Technology, Beijing 100029, China.

## Data statement

POSCAR or CONTCAR files of the optimized structures are provided into a single zip file uploaded as additional ESI.

.

